Supporting Information

Coordination-Induced p-Type Selectivity and Enhanced Hole Mobility in an Ambipolar Organic Semiconductor via Electron Passivation

Kaining Wang[a], Kun Gong[a], Kejian Jiang[a], Wenhui Feng[a], Wei Li[a], Dongzhi Liu[a*] and Xueqin Zhou[a*]

[a] School of Chemical Engineering and Technology, Tianjin University, Tianjin, 300072, P. R. China. E-mail: zhouxueqin@tju.edu.cn, dzliu@tju.edu.cn

Section S1 Synthesis and Characterization of $(TPA)_2Ab$ and $(MTPA)_2Ab$, $(MOTPA)_2Ab$, $(YD)_2Ab$

Scheme. S1 Synthetic routes of $(TPA)_2Ab$ and $(MTPA)_2Ab$, $(MOTPA)_2Ab$, $(YD)_2Ab$**.** 1: Cu, DMF, 120°C, 3 h; 2: DMF, $POCl_3$, 90 °C, 3 h; 3: *t*-BuOK, THF, rt, 2h; 4: LiCl, LiOAc, TBAB, $Pd(OAc)_2$, DMF, 120°C, 6 h, N_2; 5: $LiAlH_4$, THF, 80°C.

Synthetic details and characterization data

Materials

The reagents involved were commercially available and used without furtherpurification. All solvents were in reagent grade and were purified by the standardmethods.

1 Synthesis of 5,5'-dibromo-2,2'-dinitro-1,1'-biphenyl

2,4-dibromo-1-nitrobenzene (5.0 g, 17.8 mmol) was dissolved in DMF (20 mL) and Cu (2.70 g, 42.4 mmol) was added into the solution. The suspension was stirred andrefluxed at 120°C for 3 h and then cooled to room temperature. The precipitate was filtered and the residue was washed with 20 mL dichloromethane (DCM). The filtrate was extracted by 100 mL DCM and the combined organic phase was concentrated. The compound was purified by the column chromatography on silica gel usingcyclohexane/dichloromethane (4:1 v/v) as the eluent to yield a pale white solid (2.50 g, 70%). ^{1}H NMR ($CDCl_3$, 500 MHz)δ: 8.15(d, J=9.0 Hz, 2H), 7.76(dd, J_1=9.0 Hz, J_2=2.0 Hz, 2H), 7.48(d, J=2.0 Hz, 2H).

2 Synthesis of Aldehyde-Substituted Triarylamines (Ar-CHO)

2.1 Synthesis of 4 - (Diphenylamino)benzaldehyde

8 mL of DMF (107 mmol) was added to a 250 mL three-necked flask under a nitrogen atmosphere. After stirring at 0 °C for 10 minutes, 10 mL of $POCl_3$ was slowly and dropwise added to the DMF solution. Following the completion of the addition, the mixture was stirred at room temperature for 1 hour, during which the system turned into a white, gel-like consistency. Subsequently, 24.5 g of triphenylamine (107 mmol) was added all at once, and the temperature was gradually increased to 90 °C. The

reaction was carried out at this temperature for 3 hours. During the reaction, the color of the solution changed from yellow to dark yellow and finally to red. After cooling to room temperature, the reaction mixture was poured into 500 mL of distilled water. The pH of the solution was adjusted to neutrality using NaOH, and then it was extracted with 500 mL of dichloromethane. The organic layer was dried over anhydrous sodium sulfate, filtered, and concentrated under reduced pressure. The crude product was purified by column chromatography using a petroleum ether:ethyl acetate mixture (4:1, v/v) as the eluent. A white powder was obtained as the final product, weighing 17.8 g, with a yield of 63.5%.^{1}HNMR($CDCl_3$, 400 MHz)δ: 9.80(s, 1H), 7.67(d, J=8.4 Hz, 2H), 7.33(t, J=8.8 Hz, 4H), 7.16(d, J=8.8 Hz, 4H), 7.14(d, J=8.8 Hz, 2H), 7.12-6.98 (m, 2H).

2.2 Synthesis of 4-(N,N-Dimethoxyphenyl)aminobenzaldehyde

The synthesis was carried out following the same procedure as that for TPA-CHO, with triphenylamine replaced by N,N-di(4-methoxyphenyl)aniline (32.6 g, 107 mmol), yielding a white compound of 28.4 g with a yield of 85.4%.^{1}HNMR($CDCl_3$, 400 MHz) δ: 9.70(s, 1H), 7.51 (d, J=8.4 Hz, 2H), 7.14(d, J=8.4 Hz, 4H), 6.86(d, J=9.0 Hz, 4H), 6.84(d, J=9.4 Hz, 2H), 1.38(s, 6H).

2.3 Synthesis of 4-(p-Methylphenyl)-1,2,3,3a,4,8b-hexahydrocyclopentadeno-indole aldehyde

The synthesis was carried out following the same procedure as that for TPA-CHO, with triphenylamine replaced by 4-(p-methylphenyl)-1,2,3,3a,4,8b-hexahydrocyclopentadenoindole (26.7 g, 107 mmol), yielding a white powder of 25.6 g with a yield of 89.7%.^{1}HNMR (CDCl3, 500 MHz) δ: 9.68(s, 1H), 7.62(s, J=8.0 Hz, 1H), 7.51(d, J=8.0 Hz, 1H), 7.17-7.22(m, 4H), 6.70(d, J=9.0 Hz, 1H), 4.90(m, 1H), 3.80(m, 1H), 2.31(s, 3H), 1.48-2.14(m, 6H).

3 Synthesis of Vinyl-Substituted Triarylamine Derivatives (Ar-CH_2=CH_2)

3.1 Synthesis of 4-Methyl-N-phenyl-N-(4-vinylphenyl)aniline (TPA-CH_2=CH_2)

To a 100 mL three-necked flask were sequentially added 0.850 g of triphenylphosphine bromomethane (2.38 mmol), 0.40 g of potassium tert-butoxide (3.56 mmol), and 20 mL of tetrahydrofuran (THF). The mixture was stirred at 0 °C for

1 hour, during which the solution gradually changed in color from milky white to bright yellow. Subsequently, compound TPA-CHO (0.272 g, 1.01 mmol) was added dropwise, followed by further stirring at room temperature for 4 hours. Afterward, part of the THF was removed by rotary evaporation. The concentrated solution was poured into ice water and extracted with 500 mL of ethyl acetate. The organic layer was dried over anhydrous sodium sulfate, filtered, and concentrated under reduced pressure to afford an oily residue. Purification by column chromatography using petroleum ether as the eluent yielded a colorless transparent liquid (240 mg, 88.4% yield).[1]HNMR (CDCl3, 400 MHz) δ: 7.28(d, J=8.4 Hz, 2H), 7.24(d, J=7.6 Hz, 4H), 7.12-6.98 (m, 8H), 5.11(d, J=12 Hz,1H), 6.69-6.61 (m, 1H), 5.63 (d, J=17.6 Hz, 1H), 5.11 (d, J=12 Hz, 1H).

3.2 Synthesis of 4-Methyl-N-(p-methylphenyl)-N-(4-vinylphenyl)aniline (MTPA-CH_2=CH_2)

The reaction was carried out following the same procedure as for MTPA-CHO, with TPA-CHO replaced by MTPA-CHO (0.301 g, 1.01 mmol). A colorless transparent liquid (287 mg, 96.1% yield) was obtained after purification by column chromatography using petroleum ether as the eluent.[1]HNMR($CDCl_3$, 400 MHz) δ: 7.24(d, J=8.1 Hz, 2H), 7.05(d, J=8.1 Hz, 4H), 6.98(d, J=7.9 Hz, 4H), 6.95(s, 2H), 6.63(dd, J1=17.6 Hz, J2=10.9 Hz, 1H), 5.60(d, J=17.6 Hz, 1H), 5.11(d, J=10.9 Hz, 1H), 2.30 (s, 6H)。

3.3 Synthesis of 4-Methyl-N-(p-methoxyphenyl)-N-(4-vinylphenyl)aniline (MOTPA-CH_2=CH_2)

The reaction was carried out following the same procedure as for TPA-CH_2=CH_2, with TPA-CHO replaced by MOTPA-CHO (0.331 g, 1.01 mmol). A colorless transparent liquid (258 mg, 78.1% yield) was obtained after purification by column chromatography using petroleum ether as the eluent. [1]HNMR($CDCl_3$, 400 MHz) δ: 7.09 (d, J=8.4 Hz, 2H), 6.92 (d, J=8.8 Hz, 4H), 6.76 (d, J=8.8 Hz, 2H), 6.69 (d, J=9.2 Hz, 4H), 6.54-6.45 (m, 1H), 5.45 (2d, J=17.6 Hz,1H), 4.96 (d, J=11.2 Hz,1H), 3.64(m, 6H).

3.4 Synthesis of 4-(p-Methylphenyl)-1,2,3,3a,4,8b-hexahydrocyclopentadieno [1,2-

b]indole (YD-CH_2=CH_2)

The reaction was carried out following the same procedure as for TPA-CH_2=CH_2, with TPA-CHO replaced by YD-CHO (0.281 g, 1.01 mmol). A colorless transparent liquid (239 mg, 86.0% yield) was obtained after purification by column chromatography using petroleum ether as the eluent.[1]HNMR (500 MHz, CDCl3, δ): 7.23 (s, 1H), 7.14-7.21 (m, 4H), 7.08 (d, J = 8.5, 1H), 6.83 (d, J = 8, 1H), 6.61-6.67 (m, 1H), 5.54 (d, J = 17.5, 1H), 5.02 (d, J = 11, 1H), 4.81-4.76 (m, 1H), 3.83-3.81 (m, 1H), 2.33 (s, 3H), 1.51-2.08 (m, 6H).

4 Synthesis of Symmetrically Substituted Dinitro Biphenyl Derivatives

4.1 Synthesis of 4,4'-Bis(4-N,N'-Di(p-phenyl)aminostyryl)-4,4'-Dinitrobiphenyl ((TPA-NO_2)$_2$)

Into a 100 mL sealed flask, 5,5-dibromo-2,2'-dinitrobiphenyl (401 mg, 1.02 mmol), TPA-CH_2=CH_2 (650 mg, 2.39 mmol), palladium acetate (5.65 mg, 0.0255 mmol), lithium acetate (110 mg, 1.09 mmol), lithium chloride (125 mg, 3.01 mmol), tetrabutylammonium bromide (150 mg, 0.465 mmol), and DMF (30 mL) were added sequentially. The flask was then purged with nitrogen gas to remove oxygen, and the reaction mixture was heated to 120 ℃. During this process, the solution color gradually deepened from light yellow, indicating the progress of the reaction. The reaction was maintained at 120 ℃ for 8 hours, after which the mixture was cooled to room temperature and poured into 500 mL of ice water. The product was extracted from the aqueous phase multiple times with a small amount of ethyl acetate. After evaporation of the solvent under reduced pressure, a crude product was obtained. The crude product was then purified by column chromatography, using a mobile phase of petroleum ether: dichloromethane = 3:2 (v:v). A light red solid (384 mg) was obtained, with a yield of 49.2%. [1]HNMR($CDCl_3$, 400 MHz)δ: 8.15 (d, *J*=8.4 Hz, 4H), 7.50(d, *J*=8.4 Hz, 4H), 7.30(d, *J*=8.4 Hz, 4H), 7.24-7.18(m, 8H), 7.13(d, *J*=16 Hz, 2H), 7.05 (d, *J*=8.4 Hz, 6H), 7.02-6.96(m, 8H), 6.92(d, *J*=16.4 Hz, 2H).

4.2 Synthesis of 4,4'-Bis(4-N,N'-Di(p-methylphenyl)aminostyryl) -4,4'-Dinitro-biphenyl ((MTPA-NO_2)$_2$)

Using the same procedure as for the synthesis of (TPA-NO_2)$_2$, MTPA-CH_2=CH_2

(721 mg, 2.42 mmol) was used in place of TPA-CH_2=CH_2. A deep red compound (473 mg) was obtained, with a yield of 56.5%.^{1}HNMR ($CDCl_3$, 500 MHz) δ: 8.24 (d, *J*=8.5 Hz, 2H), 7.62 (d, *J*=8.5 Hz, 2H), 7.36-7.33 (m, 6H), 7.20-7.17 (m, 2H), 7.10-7.08 (m, 8H), 7.03-10.01 (m, 8H), 6.98-6.94 (m, 6H), 2.33 (s, 12H).

4.3 Synthesis of 4,4'-Bis(4-N,N'-Di(p-methoxyphenyl)aminostyryl) -4,4'-Dinitro-biphenyl ((MOTPA-NO_2)$_2$)

Following the same procedure as for the synthesis of (TPA-NO_2)$_2$, MOTPA-CH_2=CH_2 (795 mg, 2.42 mmol) was used instead of TPA-CH_2=CH_2. A red product (485 mg) was obtained, with a yield of 58.2%. ^{1}HNMR($CDCl_3$, 500 MHz)δ: 8.26 (d, J=8.0 Hz, 2H), 7.60 (d, J=8.0 Hz, 2H), 7.36-7.32(m, 6H), 7.20 (d, J=16.5 Hz, 2H), 7.11-7.09 (m, 8H), 6.96-6.92 (m, 2H), 6.88 (d, J=9.5 Hz, 4H), 6.85 (d, J=9.5 Hz, 8H), 3.84-3.74 (m, 12H);

4.4 Synthesis of 4,4'-Di(p-methylphenyl)-1,2,3,3a,4,8b- hexahydrocyclopentadie-noindole biphenyl ((YD-NO_2)$_2$)

Following the same procedure as for the synthesis of (TPA-NO_2)$_2$, YD-CH_2=CH_2 (660 mg, 2.41 mmol) was used in place of TPA-CH_2=CH_2. A red product (501 mg) was obtained, with a yield of 59.6%. ^{1}HNMR($CDCl_3$, 500 MHz)δ: 8.25 (d, *J*=8.5 Hz, 2H), 7.61(d, *J*=8.0 Hz, 2H), 7.36-7.32(m, 4H), 7.23-7.20(m, 2H), 7.19-7.11(m, 10H), 7.10-7.09 (m, 2H), 6.94-6.91(m, 2H), 4.85 (s, 2H), 3.86 (s, 2H), 2.35 (s, 6H), 1.49-2.14 (m, 12H);

5 Synthesis of D-A-D-Type Dipyridazine Derivatives

5.1 Synthesis of 4,4'-Bis(4-N,N'-di(p-phenyl)aminostyryl)benzo[c]quinoline ((TPA)$_2$Ab)

In a 100 mL sealed screw-cap bottle, (TPA-NO_2)$_2$ (195 mg, 0.251 mmol) and lithium aluminum hydride (400 mg, 10.0 mmol) were sequentially added to 30 mL of tetrahydrofuran (THF). The air inside the bottle was purged with nitrogen gas three times, and the reaction system was then filled with nitrogen for protection.

The reaction mixture was heated and stirred until the temperature reached 90 °C, and the reaction was maintained at 90 °C for 3 hours. After the reaction time, the process was stopped, and the mixture was cooled to room temperature.

The reaction solution was then extracted with 500 mL of ethyl acetate to collect the organic phase. After rotary evaporation of the solvent, a red solid crude product was obtained. The crude product was separated by column chromatography, using a mobile phase of dichloromethane: petroleum ether = 4:1 (v:v).Finally, a light red solid product (143 mg) was isolated, with a yield of 80.7%. ^{1}HNMR($CDCl_3$, 400 MHz) δ: 8.62(d, *J*=8.4 Hz, 2H), 8.10 (d, *J*=8.0 Hz, 2H), 7.51 (s, 2H), 7.50(d, *J*=8.4 Hz, 4H), 7.42(d, *J*=16.0 Hz, 2H), 7.33-7.28 (m, 6H), 7.15 (d, *J*=7.6 Hz, 8H), 7.10 (d, *J*=7.6 Hz, 12H);

5.2 Synthesis of 4,4'-Bis(4-N,N'-di(p-methylphenyl)aminostyryl) benzo-[c]quinoline ($(MTPA)_2Ab$)

The synthesis procedure is the same as that for $(TPA)_2Ab$, with $(TPA\text{-}NO_2)_2$ replaced by $(MTPA\text{-}NO_2)_2$ (209 mg, 0.25 mmol), yielding 164 mg of red product with a yield of 85.1%. ^{1}HNMR (DMSO-d_6, 500 MHz)δ: 8.95 (s, 2H), 8.53(d, *J*=8.5 Hz, 2H), 8.21(d, *J*=8.5 Hz, 2H), 7.62 (d, *J*=16.0 Hz, 2H), 7.53 (d, *J*=8.5 Hz, 4H), 7.43 (d, *J*=15.5 Hz, 2H), 7.13 (d, *J*=8.5 Hz, 8H), 6.90 (d, *J*=9.0 Hz, 8H), 6.90 (d, *J*=8.5 Hz, 4H), 2.26 (s, 12H).

5.3 Synthesis of 4,4'-Bis(4-N,N'-di(p-methoxyphenyl)aminostyryl) benzo[c]-quinoline ($(MOTPA)_2Ab$)

The synthesis procedure is the same as that for $(TPA)_2Ab$, with $(TPA\text{-}NO_2)_2$ replaced by $(MOTPA\text{-}NO_2)_2$ (225 mg, 0.25 mmol), yielding 182 mg of dark red product with a yield of 87.2%.^{1}HNMR (DMSO-d_6, 500 MHz)δ: 8.96 (s, 2H), 8.53 (d, *J*=8.5 Hz, 2H), 8.20 (d, *J*=8.5 Hz, 2H), 7.63 (d, *J*=16.5 Hz, 2H), 7.52 (d, *J*=8.5 Hz, 4H), 7.34 (d, *J*=16.5 Hz, 2H), 7.08 (d,*J*=8.5 Hz, 8H), 6.95 (d, *J*=8.5 Hz, 8H), 6.79 (d, *J*=8.5 Hz, 4H), 3.75 (s, 12H).

5.4 Synthesis of 4-(p-Methylphenyl)-1,2,3,3a,4,8b-hexahydrocyclo - pentadeno-indolo[c]quinoline ($(YD)_2Ab$)

The synthesis procedure is the same as that for $(TPA)_2Ab$, with $(TPA\text{-}NO_2)_2$ replaced by $(YD\text{-}NO_2)_2$ (198 mg, 0.251 mmol), yielding 164 mg of red target product with a yield of 90.1%. ^{1}HNMR (400 MHz, $CDCl_3$) δ:8.59 (d, *J* = 8.8 Hz, 2H), 8.48(s, 2H), 8.04 (d, *J* = 8.4 Hz, 2H), 7.44 (m, 2H), 7.36 (d, *J* = 16 Hz, 2H), 7.30-7.22 (m, 4H), 7.21-7.14 (m, 8H), 6.88 (d, *J* = 8.4 Hz, 2H), 4.84 (s, 2H), 3.84 (s, 2H),2.36 (s, 6H),

1.49-2.14 (m, 12H).

Section S2 Experimental Methods

^{1}HNMR: ^{1}HNMR spectra were obtained on a Varian INOVA-500MHZ superconducting spectrometer.

UV-Vis: UV-Vis Spectroscopy in solution. We obtained the absorption spectra using the Thermo Spectronic, Helios Gamma spectrometer. Quartz cells has a path length of 1 cm.

Time-Correlated Single Photon Counting (TC-SPC). Excitation of the samples was madeusingpicosecond diode lasers (NanoLED, Horiba JobinYvon Instruments) at 366 nm or 457nm, and the instrumentresponse factor was ~ 1500ps, indicating the accuracy of the instrument was ~ 150 ps. The laser's pulse energy with ca. 15 pJ was attenuated to the desired count rate of ca. 1% or less of the excitation frequency. A cooled (ca. -40°C) Hamamatsu MCP- photomultiplier R3809U 51 was employed for detecting single photons. The signal first passed through a discriminator (Ortec 9307) and then to a TAC (Ortec 566, 100 ns range used). The electrical trigger signal passed through a discriminator (Tennelec TC454) and then on to the TAC (Ortec 566). The TAC output was recorded by a DAQ-1 MCA computer card using 1024 channels then collected with HoribaJobinYvon Data Station 2.5. Measurements were done in reverse mode at 5 MHz and under magic angle polarization. A cut-off filter, GG400 with an excitation at 366nm or GG 515with an excitation at 457nm, was employed to block the stray excitation light. A dilute Ludoxsolution was used to record the instrument response function for solution measurements without any filter. No monochromator was employed, i.e. all wavelengths transmitted were recorded. The solution with a dye concentration of 5×10^{-6} mol·L^{-1} was bubbled using argon for 30 min before any measurements.

Nanosecond Transient Absorption Spectroscopy: A LP-920 laser flash photolysis Spectrometer (Edinburgh) was used to obtain the nanosecond transient absorption spectra. Excitation at 410 nm and 525 nm was directed to the sample with a power of 2.0 mJ per pulse from a computer-controlled Nd:YAG laser/OPO system from Opotek (Vibrant 355 II) operating at 10 Hz. The laser and analyzing light beam pass perpendicularly through a 1 cm quartz cell. A gated CCD camera (AndoriSTAR) was

used to obtain the time-resolved spectra.A Tektronix TDS 3012B oscilloscope and a R928P photomultiplier were used to detect the kinetic traces. The analysis was doneusing the Edinburgh analytical software (LP-920). Before the measurements, the samples in the experiments were bubbled with argon for about 30 min. The sample concentrations were 1×10^{-5} mol·L^{-1}.

Infrared: Infrared spectroscopy were obtained on a Nicokt 380 at RT.

CV: The electrochemical properties were taken using a BAS 100W electrochemical analyzer with a three-electrode configuration and a glassy carbon electrode as the working electrode, platinum as the auxiliary electrode and $Ag/AgNO_3$ electrode as the reference electrode. The instrument was calibrated with a ferrocene/ferrocenium redox couple as the external standard and a scan rate of 30 mV/s was used. The dichloromethane containing 0.1 mol·L^{-1} tetra-butylammoniumhexafluorophosphate ($TBAPF_6$) was utilized as the medium for the cyclic voltammetric determination. The concentrations of compounds were 5×10^{-3} mol·L^{-1}.

SCLC: The hole-only devices were fabricated with configuration of ITO/PEDOT:PSS/blend/Au. The electron-only devices were fabricated with a configuration of ITO/titanium (diisopropoxide) bis(2,4-pentanedionate) (TIPD)/blend/Al. The TIPD buffer layer was prepared by spin-coating a 3.5 wt % TIPD isopropanol solution onto the pre-cleaned ITO substrate and then baked at 150 ^{o}C for 10 min to convert TIPD into TOPD. Subsequently, the blend was spin-coated on it under the same condition as preparation of the optimal solar cell. The Au or Al layer was thermally deposited on the top of the blend in vacuum. The Au layer was deposited under a low speed to avoid the penetration of Au atoms into the active layer. The Al layer was deposited at a speed of 1 Å/ s. The current density voltage curves of the devices were recorded with a Keithley 2400 source.

A typical current density-voltage trace consists of four regions: region I is the Ohmic region(n=1), region II is the trap-filled region(n>3), region III is the trap-free region(n=2), and region IV is the saturation-drift region after region III, where *n* represents the slope of the fitted straight line in the logarithmic coordinate system. [1-3]

The carrier mobility μ was extracted using the Mott-Gurney law, and the fitting was

performed in the SCLC region of the J-V curve. The link between the current density and the voltage is $J_{SCLC}=9\varepsilon\varepsilon_0\mu V^2/8d^3$.The link between the trap density and the voltage of the trap-filled-limit (TFL) regime is $V_{TFL}=N_{trap}qd^2/2\varepsilon\varepsilon_0$,[4]1where q is the elementary charge (q = 1.6 x 10^{-19} C), the thickness of the material d is about 0.5 to 1 μm, $\mathcal{E}_0$ is the vacuum permittivity ($\mathcal{E}_0$ =8.854×10^{-12} F/m), and the relative permittivity $\mathcal{E}$ is 2.8 , which based on literature values of similar conjugated organic materials.[5]

EPR: The EPR measurements were carried out on a JEOL FA 200 instrument. The simulation of EPR spectra was carried out using Bruker's WIN-EPR SimFonia Software Version 1.25.

Section S3 Supplementary Figures and Tables:

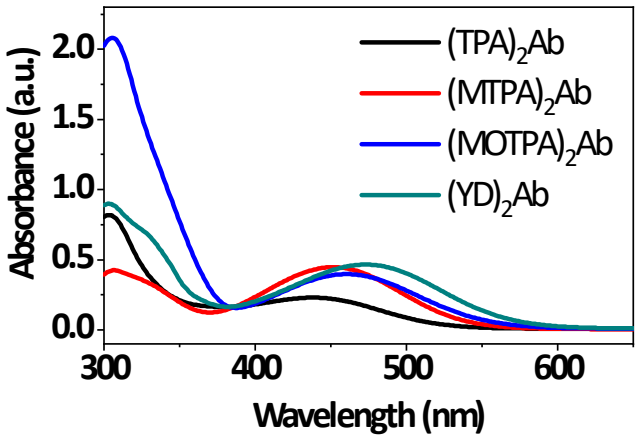

Fig. S1 UV-vis absorption of $(TPA)_2Ab$, $(MTPA)_2Ab$, $(MOTPA)_2Ab$ and $(YD)_2Ab$.

Table S1 Absorption (λ_{absmax}) and fluorescence (λ_{FLmax}) maxima, stokes shift, fluorescence lifetimes (τ_{fa}) of compounds.

Compound	λ_{abs} (nm)	λ_{FL} (nm)	Stokes shift (nm)	τ_{fa} (ns)
(TPA)2Ab	437	531	94	4.98 (4.3%) 0.34 (95.7%)
(MTPA)2Ab	450	537	87	4.18 (2.3%) 0.40 (97.7%)
(MOTPA)2Ab	462	553	91	4.55 (2.2%) 0.34 (97.8%)
(YD)2Ab	465	560	95	4.91 (1.1%) 0.35 (98.9%)

Note: The fluorescence lifetimes were measured at the emission maxima upon excited at 457 nm; The CS lifetimes were test by nanosecond transient absorption spectroscopy.

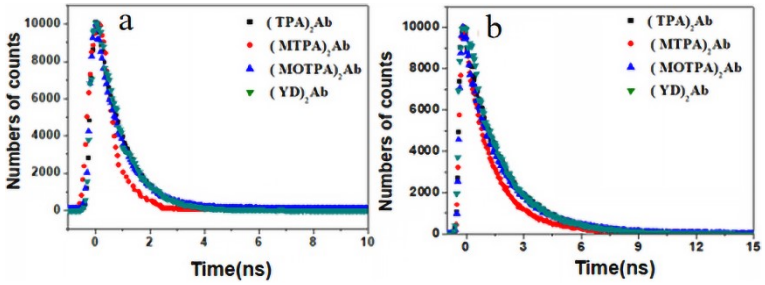

Fig. S2 Time-resolved fluorescence spectra of $(TPA)_2Ab$, $(MTPA)_2Ab$, $(MOTPA)_2Ab$ and $(YD)_2Ab$. The excitation wavelength is at 366 nm (a) and 457 nm (b), respectively.

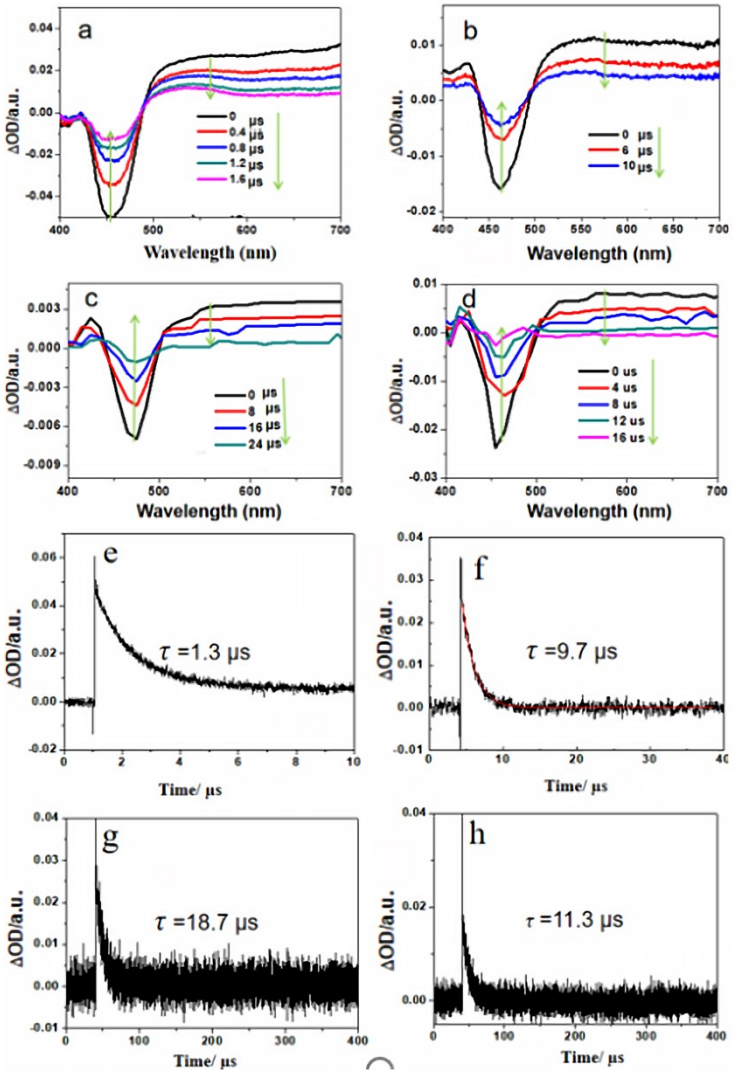

Fig. S3 Nanosecond transient absorption spectra and the decay kinetics of the radical cations at 530 nm by the nanosecond transient absorption spectra of $(TPA)_2Ab$ (a, e), $(MTPA)_2Ab$, (b, f), $(MOTPA)_2Ab$ (c, g) and $(YD)_2Ab$ (d, h).

Table S2 Trap state densities and mobilities of the ambipolar and $PtCl_4$ complexes.

Compound	Hole transport			Electron transport		
	μ_h	V_{TFL}	N_{trap}	μ_e	V_{TFL}	N_{trap}
	$cm^2 \cdot V^{-1}s^{-1}$	V	cm^{-3}	$cm^2 \cdot V^{-1}s^{-1}$	V	cm^{-3}
$(TPA)_2Ab$	3.4×10^{-5}	2.22	5.50×10^{16}	1.4×10^{-5}	0.90	2.23×10^{16}
$[(TPA)_2Ab]PtCl_4$	3.9×10^{-3}	0	0	4.1×10^{-7}	2.99	7.41×10^{16}
$(MTPA)_2Ab$	3.3×10^{-4}	3.30	8.18×10^{16}	4.5×10^{-5}	0.85	2.11×10^{16}
$[(MTPA)_2Ab]PtCl_4$	8.2×10^{-2}	0	0	4.9×10^{-6}	1.42	3.52×10^{16}
$(MOTPA)_2Ab$	7.2×10^{-5}	2.41	5.98×10^{16}	1.9×10^{-3}	1.11	2.75×10^{16}
$[(MOTPA)_2Ab]PtCl_4$	1.6×10^{-4}	0	0	8.7×10^{-5}	4.26	1.06×10^{16}
$(YD)_2Ab$	8.7×10^{-5}	2.14	5.31×10^{16}	8.9×10^{-4}	0.87	2.15×10^{16}
$[(YD)_2Ab]PtCl_4$	4.9×10^{-3}	0	0	1.9×10^{-6}	1.10	2.93×10^{16}

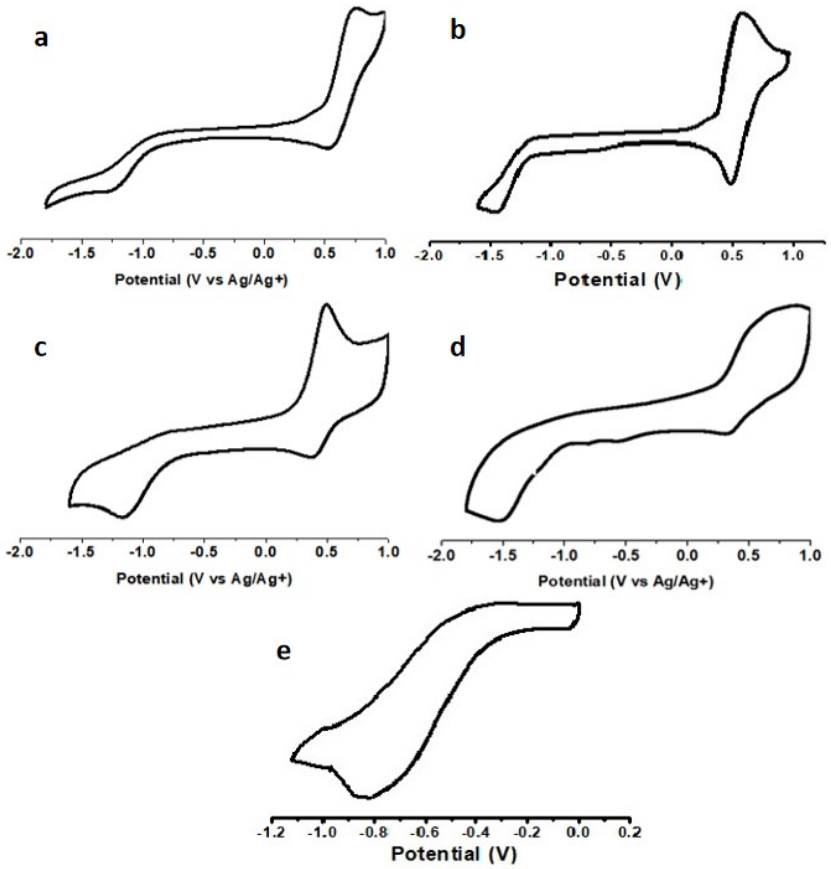

Fig. S4 Electrochemical curves of (a) $(TPA)_2Ab$ (b) $(MTPA)_2Ab$ (c) $(MOTPA)_2Ab$ (d) $(YD)_2Ab$ (e) $PtCl_4$ vs Ag/Ag+, with the concentration of 5×10^{-3} mol•L^{-1}.

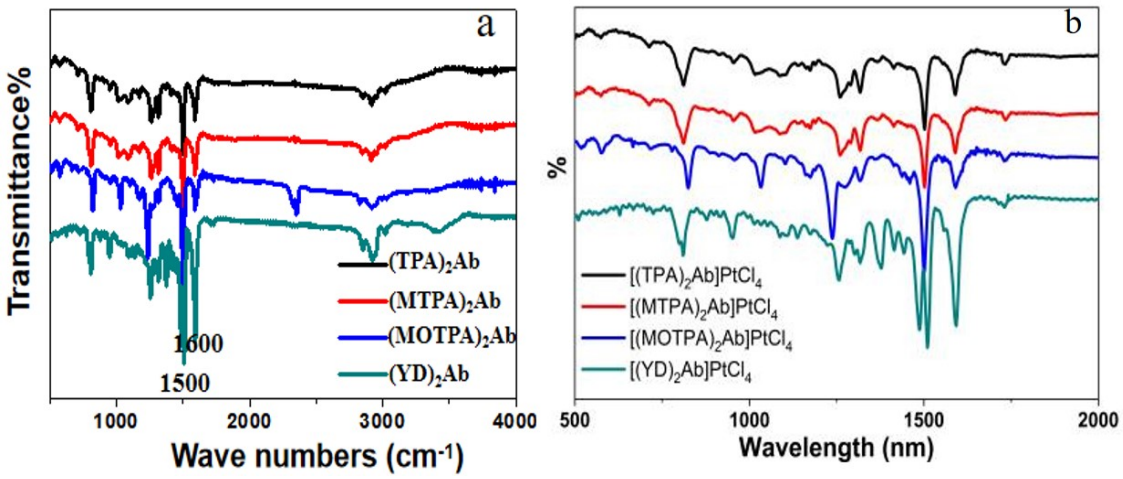

Fig. S5 Infrared spectra of (a) $(Ar)_2Ab$ and (b) $[Ar_2Ab]PtCl_4$.

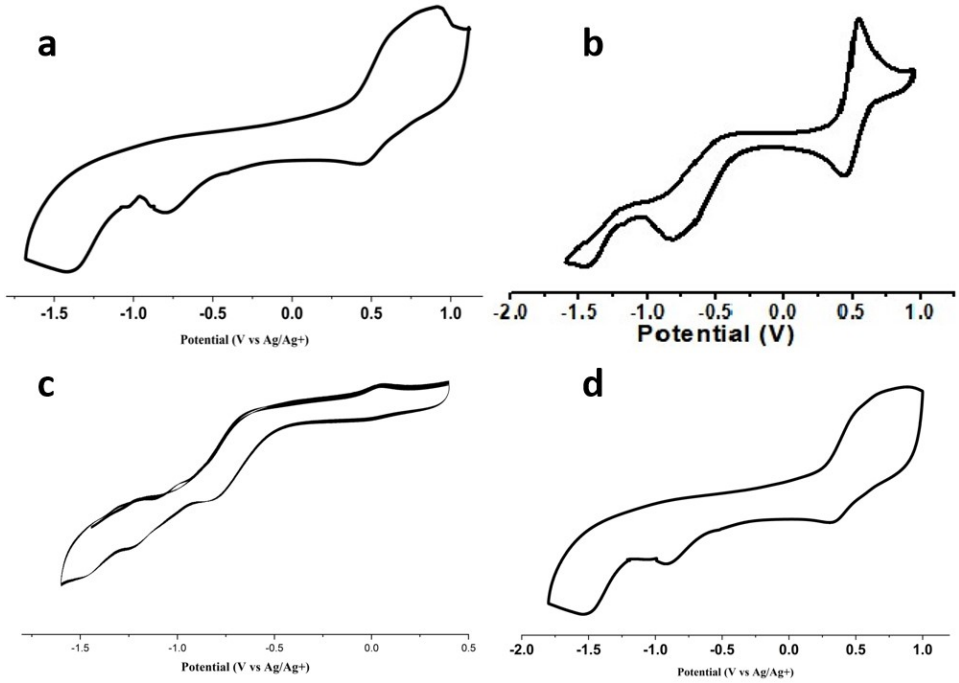

Fig. S6 Electrochemical curves of (a) $[(TPA)_2Ab]PtCl_4$ (b)[$(MTPA)_2Ab]PtCl_4$ (c) $[(MOTPA)_2Ab]PtCl_4$ (d) $[(YD)_2Ab]PtCl_4$ vs Ag/Ag+, with the concentration of 5×10^{-3} mol•L^{-1}.

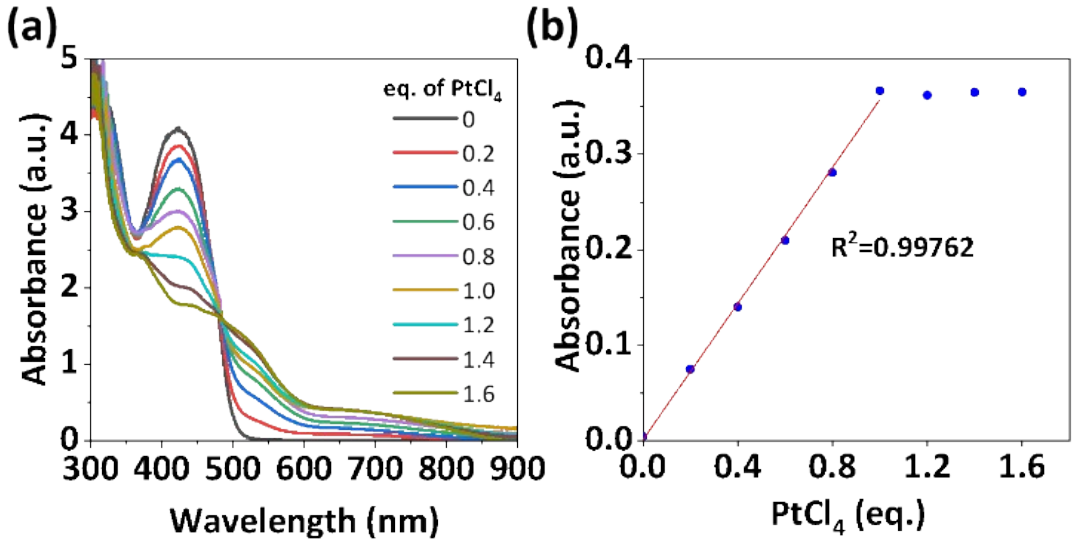

Fig. S7 (a) Absorption spectra of $(TPA)_2Ab$ upon addition of $PtCl_4$ (0-1.6 eq.). (b)The absorption intensity at 700 nm correlates with the concentration of $PtCl_4$ solution in a specific curve.

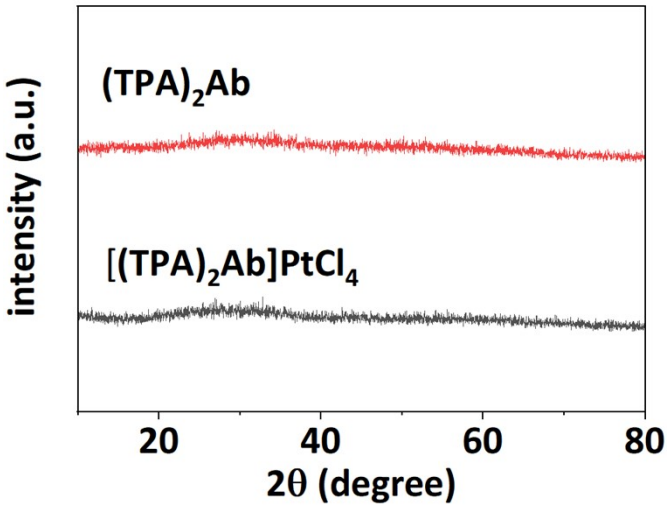

Fig. S8 XRD spectra of (TPA)2Ab and $[(TPA)_2Ab]PtCl_4$

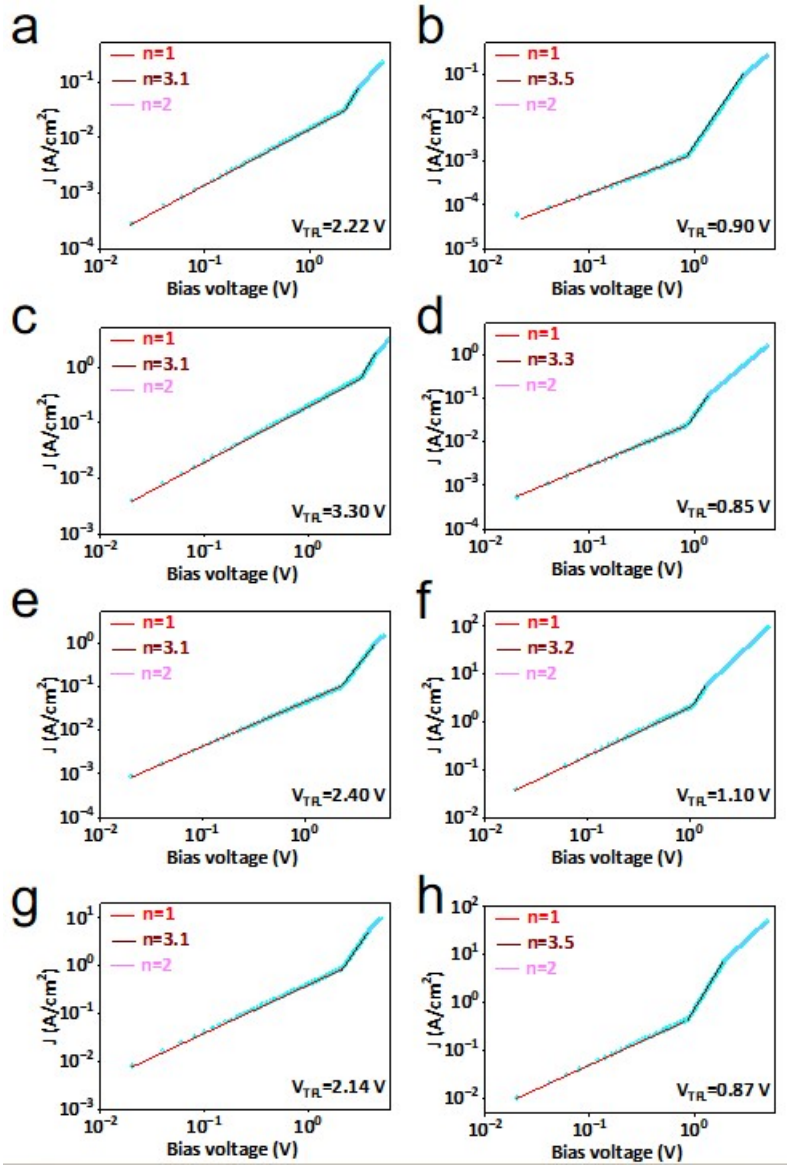

Fig. S9 J-V curve of $(TPA)_2Ab$ (a, b), $(MTPA)_2Ab$ (c, d), $(MOTPA)_2Ab$ (e, f) and $(YD)_2Ab$ (g, h) by SCLC technique, where a, c, e and g are hole-dominated devices, and b, d, f and h are electron-dominated devices.

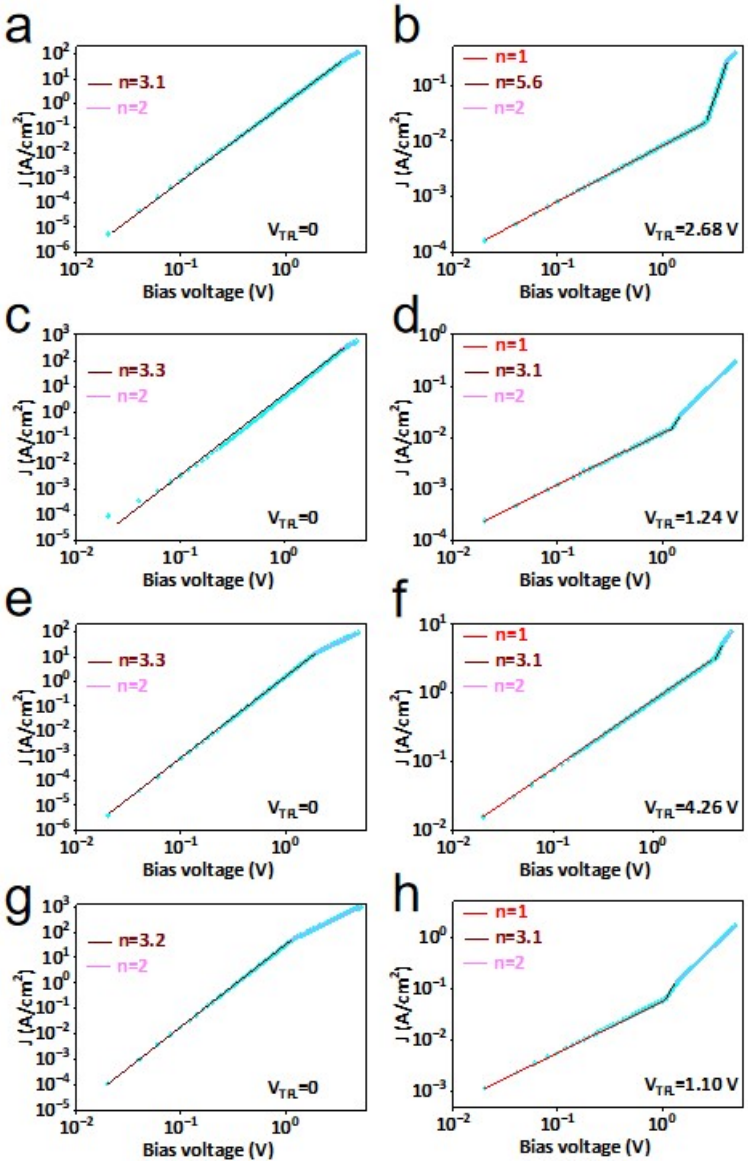

Fig. S10 J-V curve of 365nm ultraviolet light-treated $[(TPA)_2Ab]PtCl_4$ (a, b), $[(MTPA)_2Ab]PtCl_4$ (c, d), $[(MOTPA)_2Ab]PtCl_4$ (e, f) and $[(YD)_2Ab]PtCl_4$ (g, h) by SCLC technique, where a, c, e and g are hole-dominated devices, and b, d, f and h are electron-dominated devices.

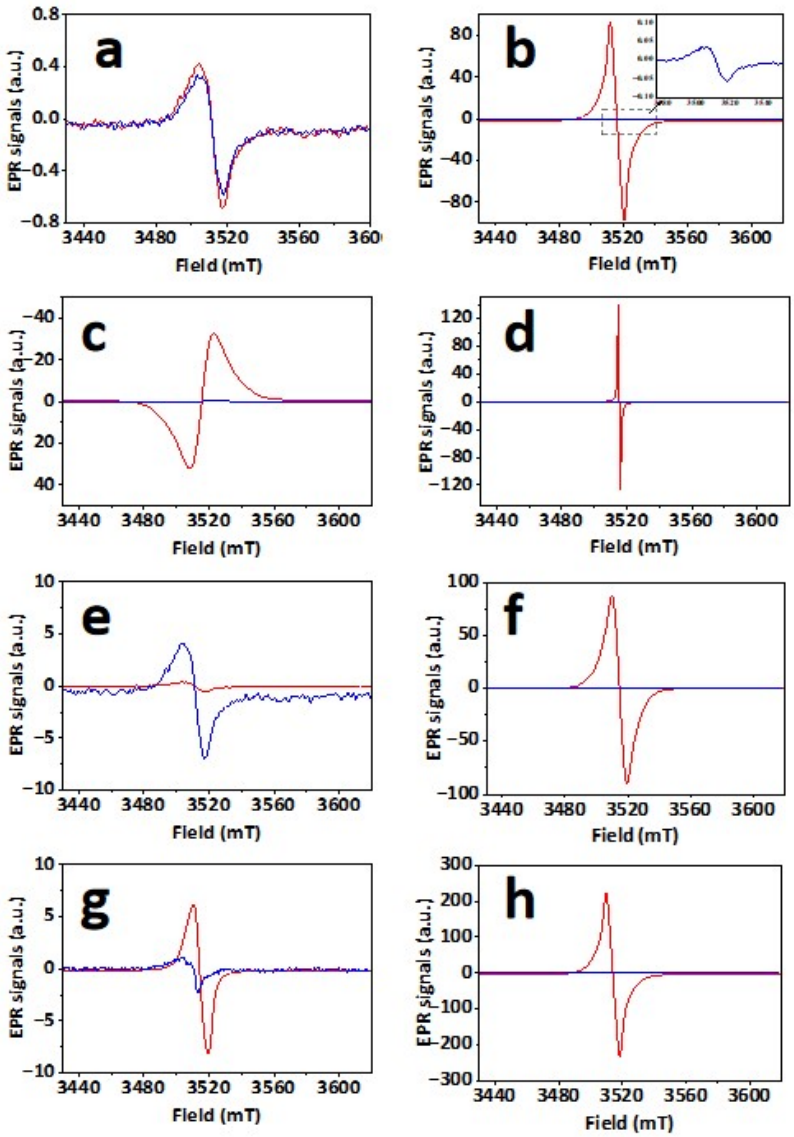

Fig. S11 ESR spectra of $(TPA)_2Ab$ (a), $(MTPA)_2Ab$ (c) , $(MOTPA)_2Ab$ (e) and $(YD)_2Ab$ (g) and their complexes with $PtCl_4$ (b, d, f, h). The red lines represent hole signals, and the blue lines represent electron signals.

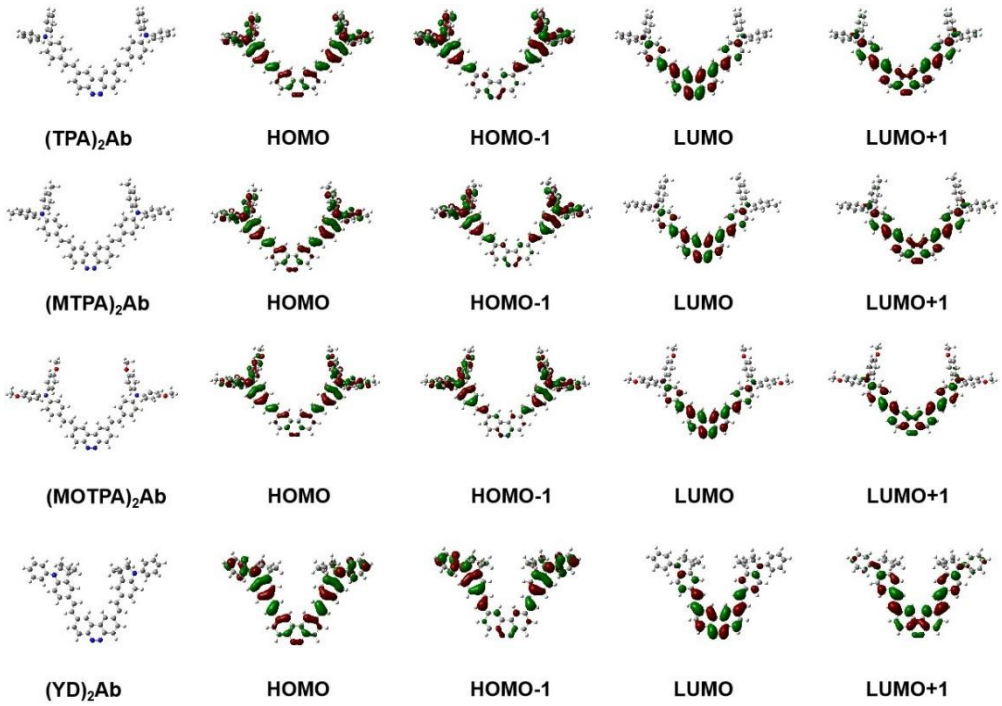

Fig. S12 Molecular structure and orbitals of $(TPA)_2Ab$, $(MTPA)_2Ab$, $(MOTPA)_2Ab$ and $(YD)_2Ab$.

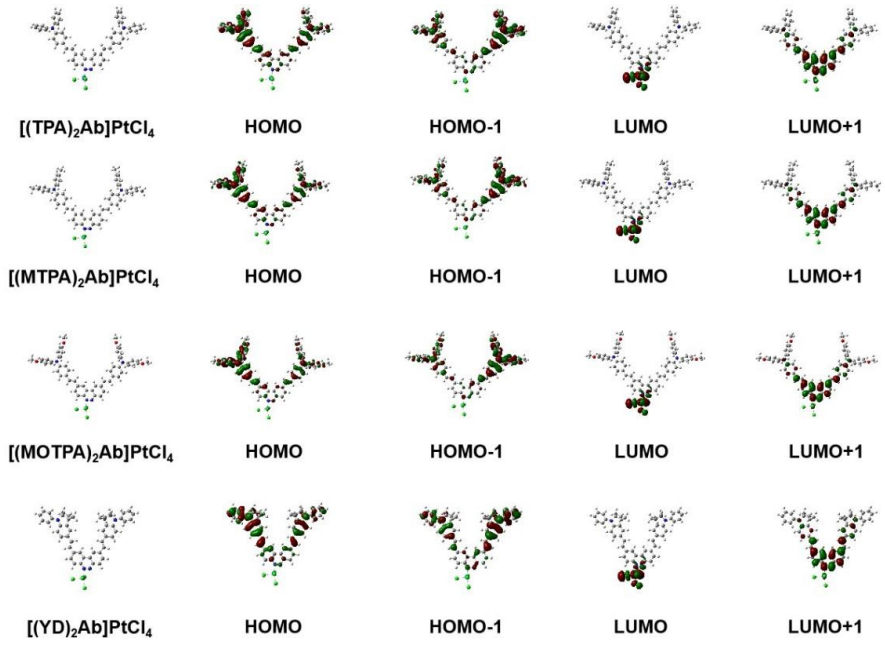

Fig. S13 Molecular structure and orbitals of $[(TPA)_2Ab]PtCl_4$, $[(MTPA)_2Ab]PtCl_4$, $[(MOTPA)_2Ab]PtCl_4$ and $[(YD)_2Ab]PtCl_4$. The N-Pt bond lengths in sequence are 2.09725, 2.09610, 2.09466, 2.09666.

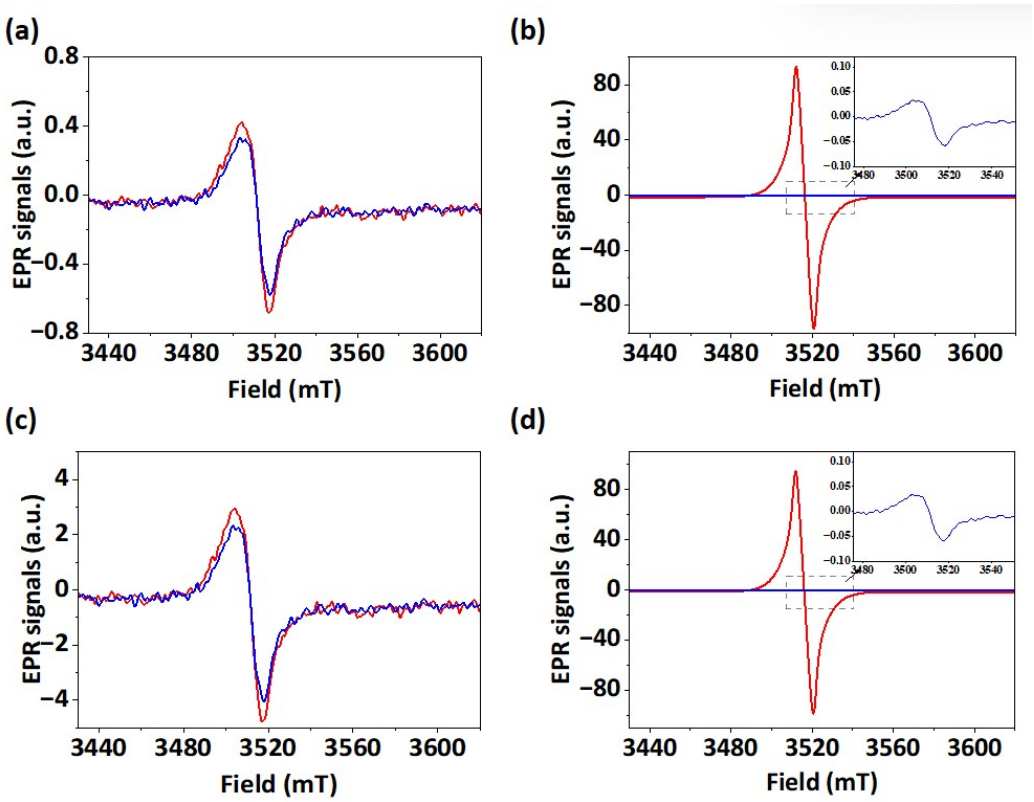

Fig. S14 ESR spectra of $(TPA)_2Ab$ (a,c) and $[(TPA)_2Ab]PtCl_4$ (b,d), where the red line represents the hole signals and the blue line is the electron signals.powders under dark(a,b) and exposure to light (c,d).

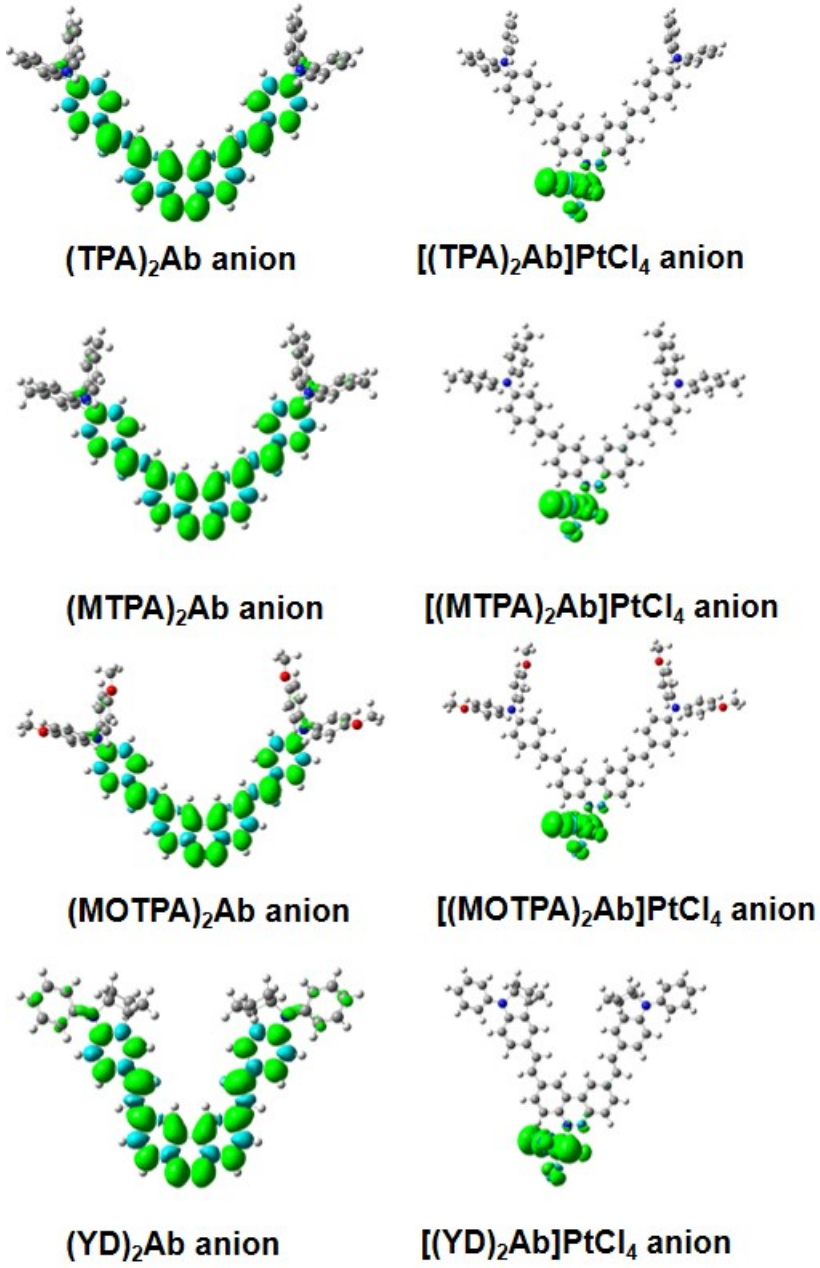

Fig. S15 Spin density distribution of $(Ar)_2Ab$ and $[(Ar)_2Ab]PtCl_4$.

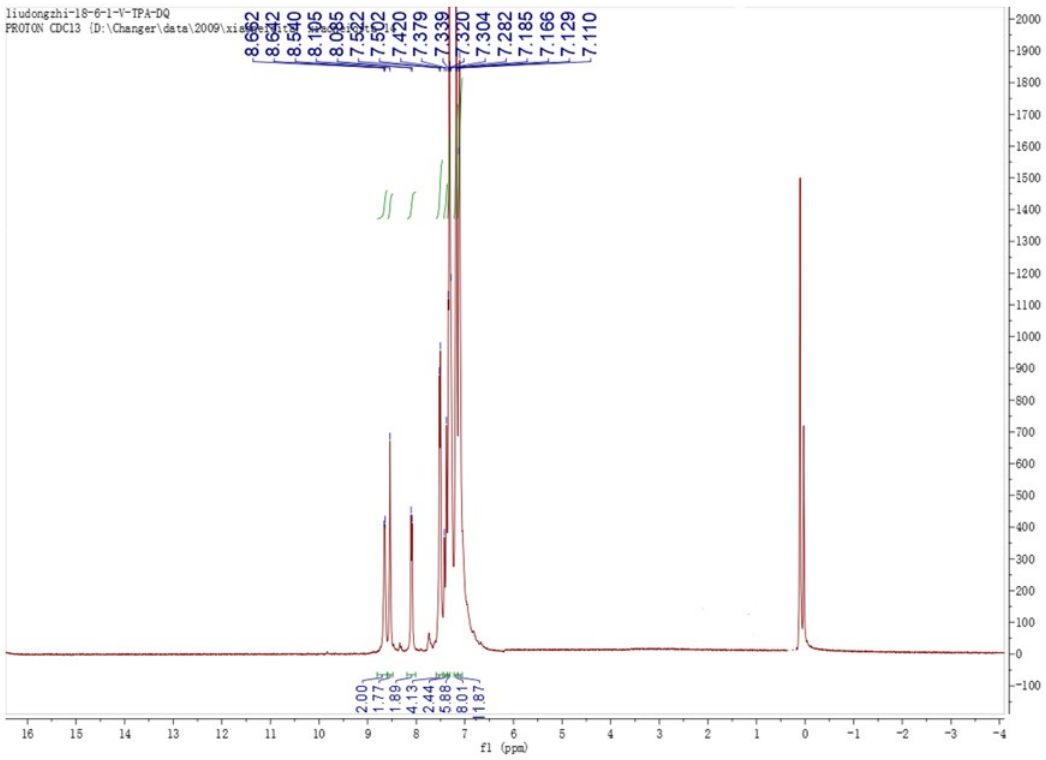

Fig. S16 400 MHz ^{1}H NMR spectrum of $(TPA)_2Ab$.

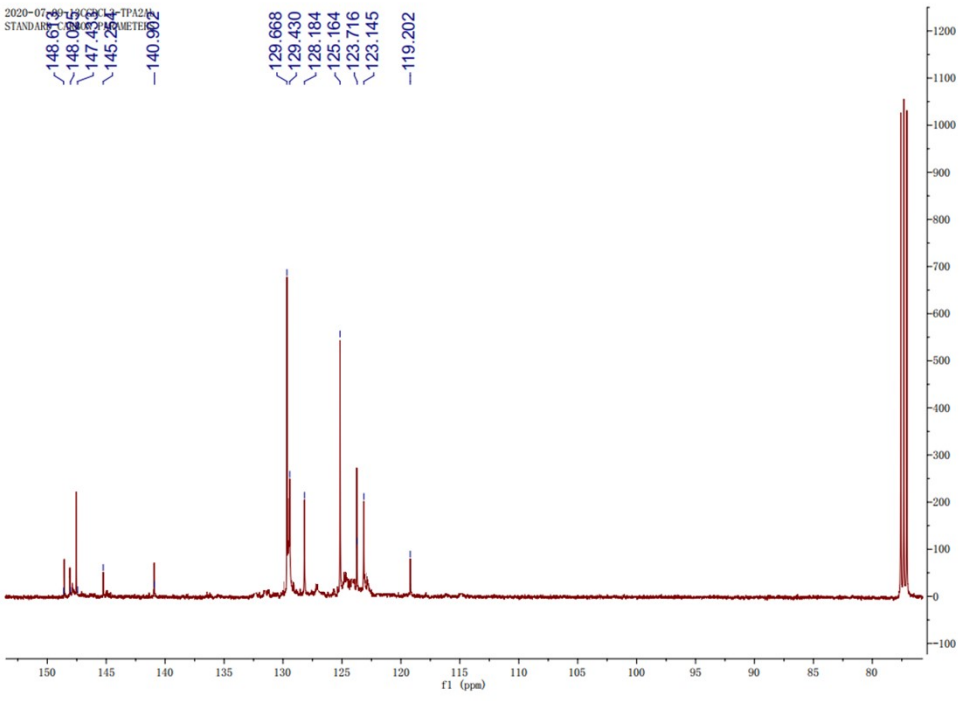

Fig. S17. 500 MHz ^{13}C NMR spectrum of $(TPA)_2Ab$.

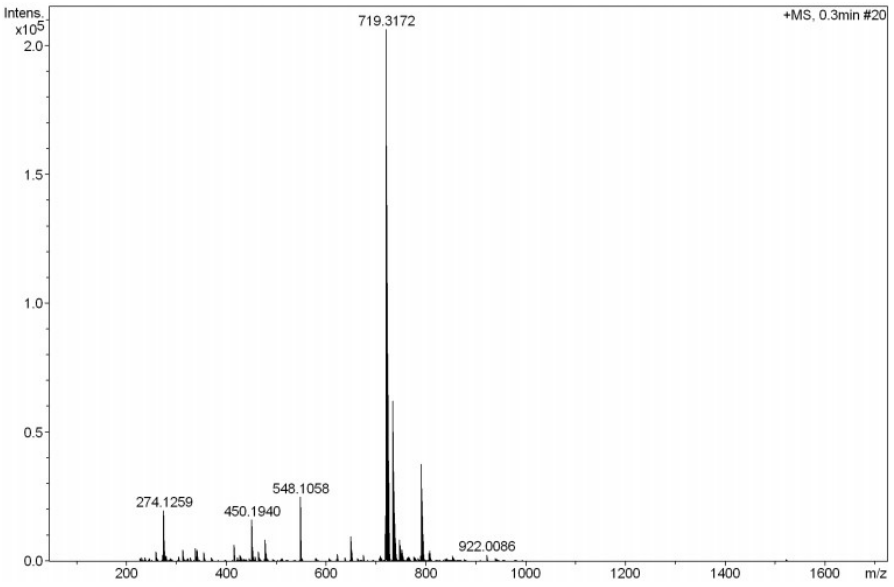

Fig. S18. HRMS (APCI) spectrum of $(TPA)_2Ab$. $[M+H]^+$calculated for $C_{52}H_{39}N_4^+$: 719.3171, found: 719.3172.

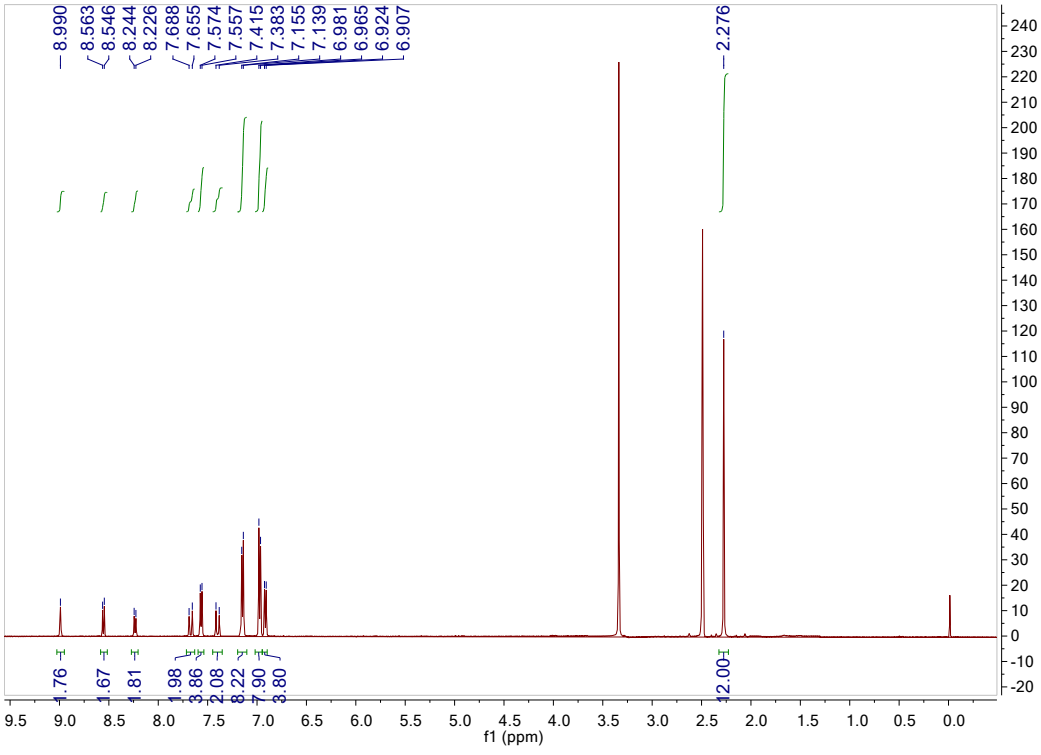

Fig. S19. 500 MHz ^{1}H NMR spectrum of $(MTPA)_2Ab$**.**

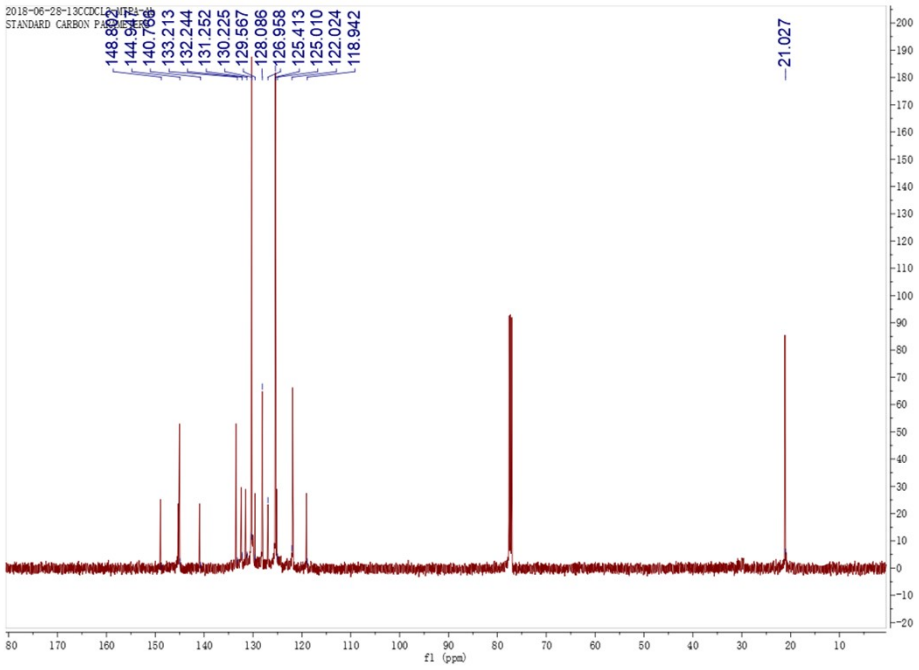

Fig. S20. 500 MHz ^{13}C NMR spectrum of $(MTPA)_2Ab$.

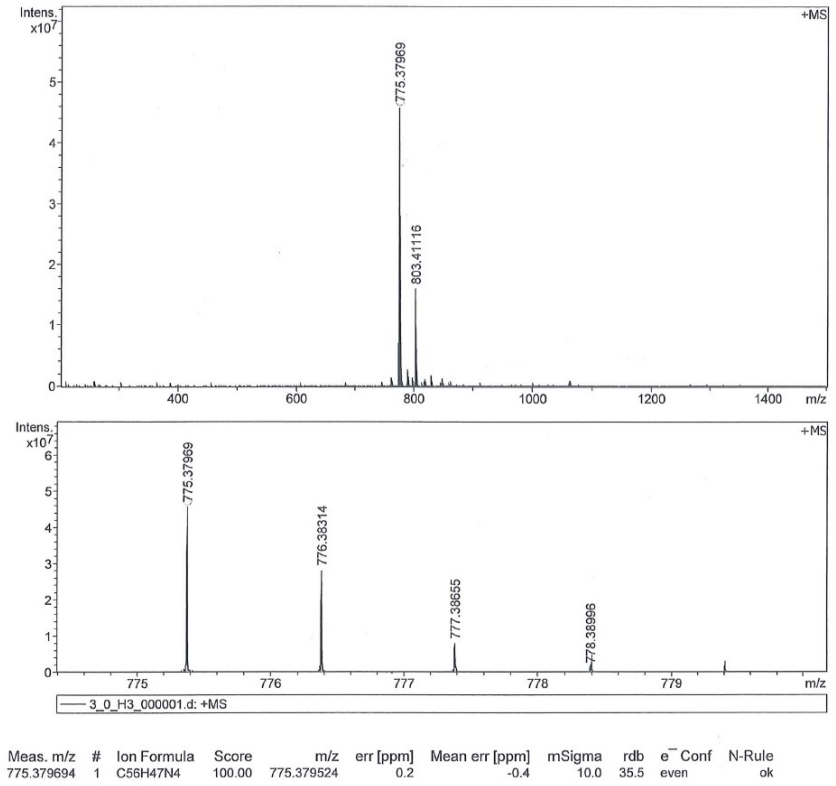

Fig. S21. HRMS (APCI) spectrum of $(MTPA)_2Ab$. (m/z): $[M+H]^+$calculated for calculated for $C_{56}H_{47}N_4$: 775.3795, found: 775.3796.

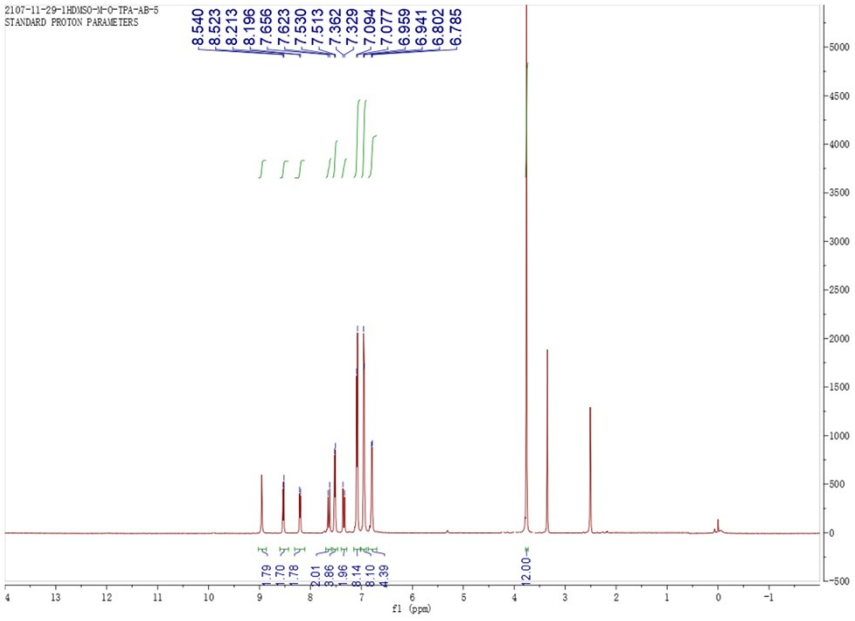

Fig. S22. 500 MHz ^{1}H NMR spectrum of $(MOTPA)_2Ab$.

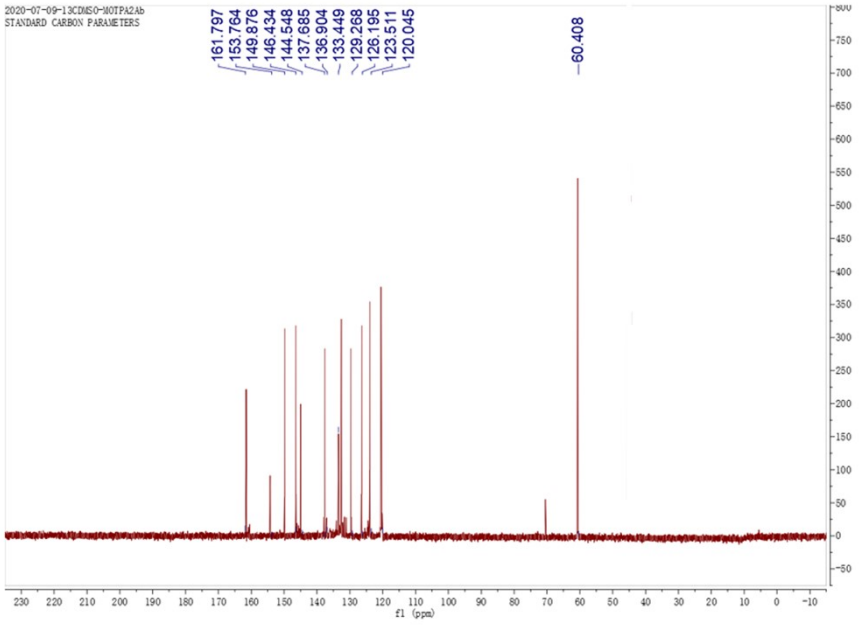

Fig. S23. 500 MHz ^{13}C NMR spectrum of $(MOTPA)_2Ab$.

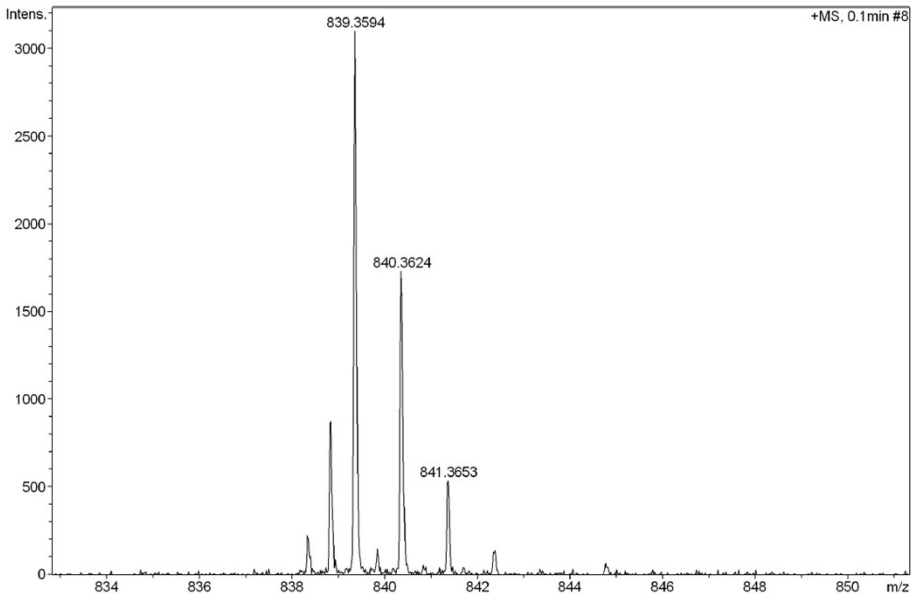

Fig. S24. HRMS (APCI) spectrum of $(MOTPA)_2Ab$.

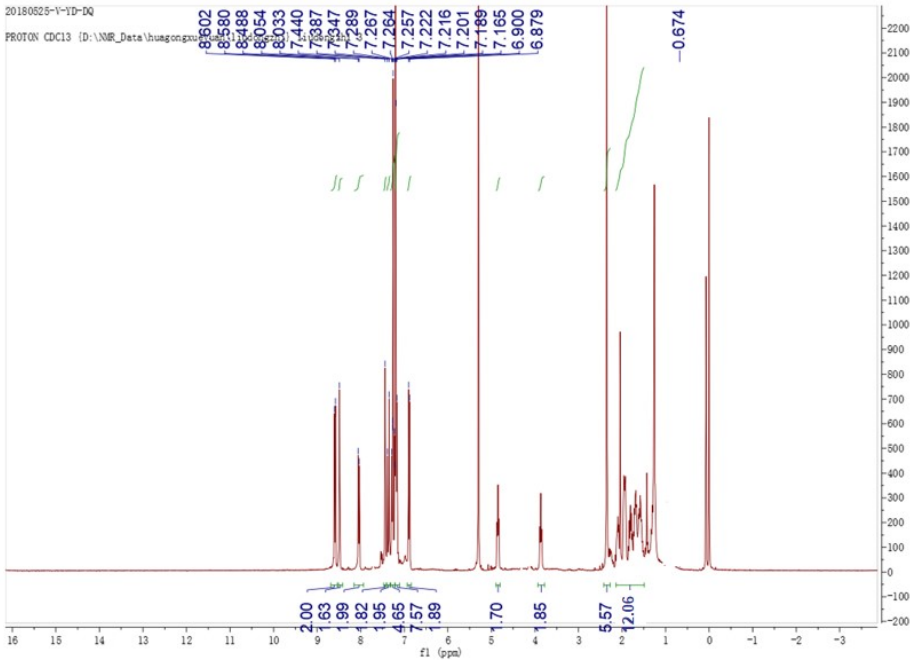

Fig. S25. 400 MHz ^{1}H NMR spectrum of $(YD)_2Ab$.

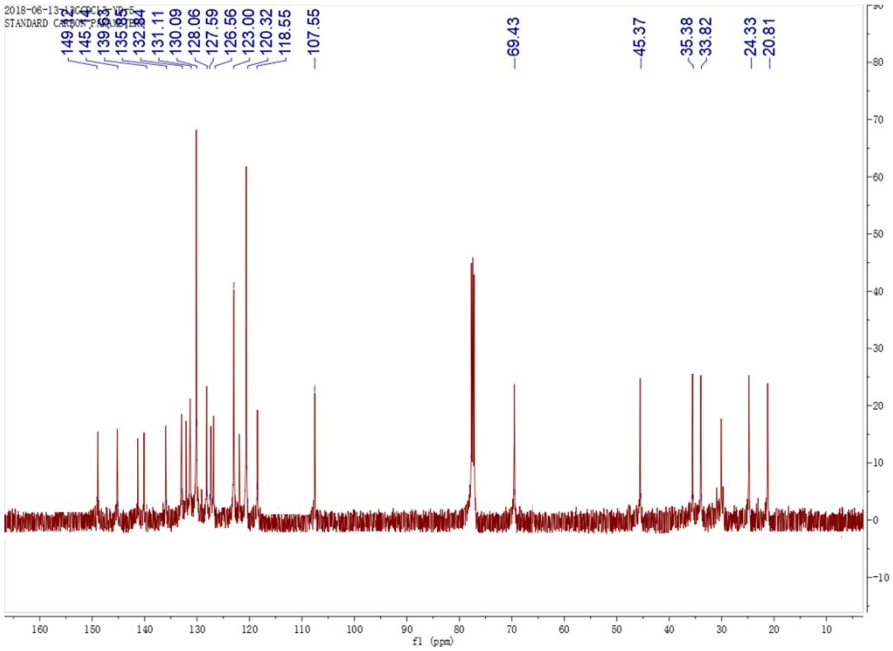

Fig. S26. 500 MHz ^{13}C NMR spectrum of $(YD)_2Ab$.

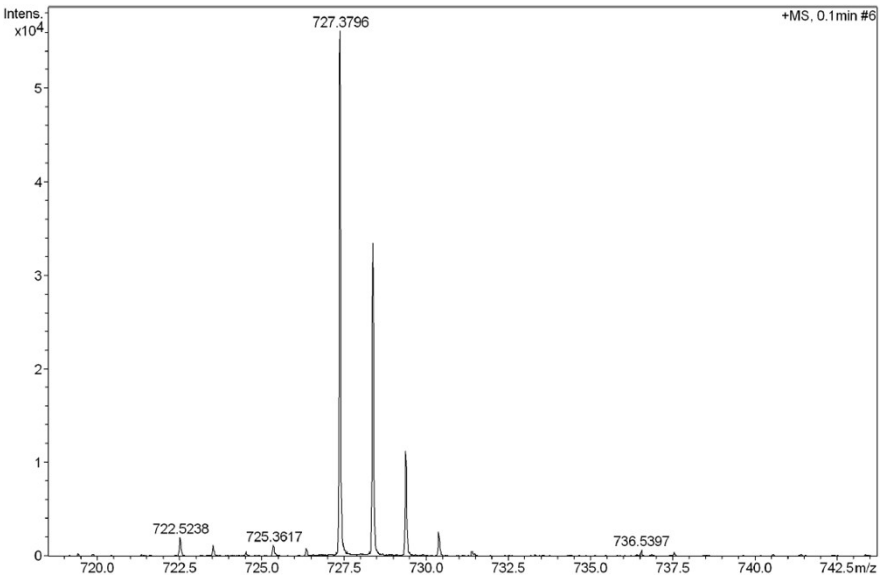

Fig. S27. HRMS(APCI) spectrum of $(YD)_2Ab$.

Table S3 Mobilities of representative p-type organic semiconductors.

Material	**Hole Mobility ($cm^2/V·s$)**	**Preparation Method**	**Film Morphology**	**Test Method**
Pentacene[6]	1~5.5	Vacuum deposition	Single crystal	FET
C8-BTBT[7]	1.4~10.4	Vacuum deposition	Single crystal	FET
DNTT[8]	2~3	Spin coating	Single crystal	FET
Spiro-OMeTAD[9]	10^{-5}~10^{-2}	Spin coating	Thin film	SCLC
P3HT[10]	10^{-4}~10^{-3}	Spin coating	Thin film	SCLC
PEDOT:PSS[11]	10^{-4}~10^{-5}	Spin coating	Conductive polymer	SCLC
PTAA[12]	10^{-6}~10^{-3}	Spin coating	Thin film	SCLC

Section S4 Computational Details

All the calculations were carried out using Gaussian 16, Revision A.03 codes under[13] the of density functional theory (DFT) framework. The ground state geometries of the species were fully optimized at B3LYP[14, 15] /def2-SVP level in vacuo. Vibrational frequency calculations for all the optimized geometries were performed at the same level to ensure the structures correspond to the local minima on the potential energy surface. The spin densities of the cation and anion radicals were calculated by removing or adding an electron to the neutral systems using the unrestricted DFT (UDFT) method.

Section S5 References

1. M. Ghorab, A. Fattah and M. Joodaki, *Optik*, 2022, **267**, 169730.
2. Z. An, J. Yu, S. C. Jones, S. Barlow, S. Yoo, B. Domercq, P. Prins, L. D. A. Siebbeles, B. Kippelen and S. R. Marder, *Adv. Mater.*, 2005, **17**, 2580-2583.
3. V. D. Mihailetchi, J. K. J. van Duren, P. W. M. Blom, J. C. Hummelen, R. A. J. Janssen, J. M. Kroon, M. T. Rispens, W. J. H. Verhees and M. M. Wienk, *Adv. Funct. Mater.*, 2003, **13**, 43-46.
4. X. de Vries and R. Coehoorn, *Physical Review Materials*, 2020, **4**.
5. D. Shi, V. Adinolfi, R. Comin, M. Yuan, E. Alarousu, A. Buin, Y. Chen, S. Hoogland, A. Rothenberger, K. Katsiev, Y. Losovyj, X. Zhang, P. A. Dowben, O. F. Mohammed, E. H. Sargent and O. M. Bakr, *Science*, 2015, **347**, 519-522.
6. M. Kitamura and Y. Arakawa, *Journal of Physics: Condensed Matter*, 2008, **20**.
7. L. Wang, C. Gao, S. Ruan, J. Yang, S. Liang, C. Yang and W. Li, *IEEE Electron Device Letters*, 2024, **45**, 1949-1952.
8. U. Kraft, K. Takimiya, M. J. Kang, R. Rödel, F. Letzkus, J. N. Burghartz, E. Weber and H. Klauk, *Org. Electron.*, 2016, **35**, 33-40.
9. M. Hatamvand, P. Vivo, M. Liu, M. Tayyab, D. Dastan, X. Cai, M. Chen, Y. Zhan, Y. Chen and W. Huang, *Vacuum*, 2023, **214**.
10. F. Laquai, D. Andrienko, R. Mauer and P. W. Blom, *Macromol Rapid Commun*, 2015, **36**, 1001-1025.
11. Z. Shariatinia, *Renewable and Sustainable Energy Reviews*, 2020, **119**.
12. H. D. Pham, T. C. J. Yang, S. M. Jain, G. J. Wilson and P. Sonar, *Advanced Energy Materials*, 2020, **10**.
13. M. J. Frisch, G. W. Trucks, H. B. Schlegel, G. E. Scuseria, M. A. Robb, J. R. Cheeseman, G. Scalmani, V. Barone, G. A. Petersson, H. Nakatsuji, X. Li, M. Caricato, A. V. Marenich, J. Bloino, B. G. Janesko, R. Gomperts, B. Mennucci, H. P. Hratchian, J. V. Ortiz, A. F. Izmaylov, J. L. Sonnenberg, D. Williams-Young, F. Ding, F. Lipparini, F. Egidi, J. Goings, B. Peng, A. Petrone, T. Henderson, D. Ranasinghe, V. G. Zakrzewski, J. Gao, N. Rega, G. Zheng, W. Liang, M. Hada, M. Ehara, K. Toyota, R. Fukuda, J. Hasegawa, M. Ishida, T. Nakajima, Y. Honda, O. Kitao, H. Nakai, T. Vreven, K. Throssell, J. A. Montgomery, Jr., J. E. Peralta, F. Ogliaro, M. J. Bearpark, J. J. Heyd, E. N. Brothers, K. N. Kudin, V. N. Staroverov, T. A. Keith, R. Kobayashi, J. Normand, K. Raghavachari, A. P. Rendell, J. C. Burant, S. S. Iyengar, J. Tomasi, M. Cossi, J. M. Millam, M. Klene, C. Adamo, R. Cammi, J. W. Ochterski, R. L. Martin, K. Morokuma, O. Farkas, J. B. Foresman, and D. J. Fox, Gaussian 16, Revision A.03, Gaussian, Inc., Wallingford CT, 2016.
14. A. D. Becke, *J. Chem. Phys.*, 1993, **98**, 5648-5652.
15. C. Lee, W. Yang and R. G. Parr, *Phys. Rev. B*, 1988, **37**, 785-789.